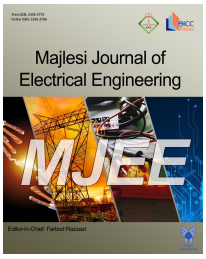

Volume 18, Issue 3, 182449 (1-7)

Majlesi Journal of Electrical Engineering (MJEE)

https://dx.doi.org/10.57647/j.mjee.2024.180349

Efficiency enhancement of a tandem Perovskite-Silicon solar cell

Akram Akbari[1], Sayyed-Hossein Keshmiri[2]

[1]*Department of Electrical Engineering, Bojnourd Branch, Islamic Azad University, Bojnourd, Iran.*
[2]*Electrical Engineering Department, Faculty of Engineering, Ferdowsi University, Mashhad, Iran.*

*Corresponding author: keshmiri@um.ac.ir

Original Research

Received:
27 June 2024
Revised:
6 August 2024
Accepted:
20 August 2024
Published online:
3 September 2024

Abstract:

A tandem solar cell consisting of three cells is designed and simulated by the Solar Cell Capacitor Simulator (SCAPS) program. The bandgap of the top cell absorber ($Cs_2AgBi_{0.75}Sb_{0.25}Br_6$) is 1.8 eV, the middle cell absorber ($CH_3NH_3PbI_3$) has a bandgap of 1.55 eV), and a single-crystal silicon cell (with 1.12 eV bandgap) is selected as the bottom cell. Each of these cells were simulated and optimized separately. To improve current density in the middle cell, CuSCN is chosen as the hole-transport layer (HTL). Power conversion efficiencies (PCE) of individual $Cs_2AgBi_{0.75}Sb_{0.25}Br_6$, $MAPbI_3$, and Si cells are 14.32%, 25.09%, and 25.22%, respectively. which are quite close to the results published in the literature. Consequently, the tandem structure of these cells is simulated and the optimal thicknesses for the absorber layers (as required by the current-matching condition) in a two-terminal (2T) monolithic structure is calculated. The optimized thicknesses of $Cs_2AgBi_{0.75}Sb_{0.25}Br_6$ and $MAPbI_3$ absorber layers in the tandem configuration are 300 and 550 nm, respectively. The transmitted spectra of the top and middle cells are obtained using the Matlab software. Subsequently, the SCAPS numerical simulation for the 2T tandem structure gave an enhanced power conversion efficiency (PCE) of 38.9%.

Keywords: Photovoltaic solar cells; Tandem structure; Perovskite solar cells; PCE enhancement.

1. Introduction

Perovskite absorber layers have shown good optoelectronics properties, such as adjustable bandgaps, high absorption coefficients, relatively long carrier lifetimes, rather high electron and hole mobilities, and fairly small exciton binding energies [1]. These characteristics are suitable for single-junction solar cells, as well as for tandem structures.

Using a tandem solar device structure is an effective approach to bypass the Shockley-Queisser limit of 31% efficiency in single-junction solar cells [1, 2]. The two most significant mechanisms of power loss in single-junction cells are: 1) photons with energies lower than the bandgap are not absorbed; and 2) photons with energies higher than the bandgap lose part of their energies as heat (i.e. thermal losses). Typically, these two mechanisms account for the loss of almost half of the ideal solar cell efficiency. Consequently, tandem cells can be designed to partly compensate for these shortcomings [3]. In a tandem solar cell, the top cell (which has a wider bandgap) absorbs higher-energy photons, and the photons with lower energies pass through it to be absorbed by the next cell, and so on. In this way, an enhanced absorption of sunlight is attainable.

Tandem solar cells of organic-inorganic halide perovskite semiconductors on silicon (Si) have the advantages of low fabrication costs and high efficiencies (due to the bandgap tunability of the perovskite materials, ranging from 1.3 eV to 2.1 eV) [2]. These cells can be designed as a monolithic structure which is a two-terminal (2T) structure, or as a mechanical stack which with four terminals (i.e. 4T structure). The 2T architecture is less expensive to build; it only needs one transparent-conductive electrode inside the device, which results in saving materials and reducing the optical losses of the interface layer between subcells (as compared to the 4T cells); and also, the wiring of the cell would be easier. Furthermore, it requires a lower processing temperature.

In recent years, a lot of research has been done on increas-

ing the stability and conversion efficiency of perovskite solar cells. The PCE of single-junction perovskite solar cells is improved to around 25% and its fabrication cost is decreased significantly; especially with the production of carbon-based perovskite solar cells [4]. Recently, high efficiency and improved stability of solar cells based on $MAPbI_3$ were demonstrated [5].

The first two-terminal perovskite-silicon tandem cell was fabricated by producing an n+-doped tunnel junction between the thin-film perovskite and single-crystal Si cells. This structure resulted in a 13.7% efficiency [6]. In another work, a SnO_2 film was used as an electron-transport layer (ETL) for the perovskite cell; it was deposited by the atomic-layer deposition (ALD) technique at a temperature below 120 ^oC. With this structure, 18.1% efficiency was obtained [7]. Werner et al. fabricated a monolithic perovskite-Si heterojunction tandem cell using an indium-zinc oxide (IZO) layer as an intermediate recombination layer; and after optimization of the hole-transport layer (HTL) thickness, they reached 19.2% efficiency [8]. Shen et al. designed a 2T tandem device with a TiO_2 layer (as the electron transport and recombination layer), deposited by ALD technique. They reached PCEs of 22.9% (for the homojunction) and 24.1% (for the heterojunction) cells [9].

Another 2T tandem solar cell with a PCE of 23.6% was reported by Bush et al. [10]. They used a bilayer of SnO_2 (4 nm) and zinc-tin oxide (2 nm) deposited by a ALD technique (at low-temperature). These layers prevented the perovskite layer from being damaged during the ITO sputtering process, and also enhanced the thermal and environmental stability of the tandem cell. The thickness of the front ITO layer was reduced, in order to decrease its parasitic absorption and reflection. They chose a perovskite layer with a bandgap of 1.68 eV as the front cell, and used PTAA as the HTL (instead of NiOx); consequently, the PCE of the cell was increased to 25% [11]. Sahli et al. used a nanocrystalline silicon recombination junction in a textured perovskite-on-Si tandem cell and obtained a PCE of 25.2% [12, 13]. Xu et al. used Cl, Br, and I alloys to attain a perovskite bandgap of 1.67 eV. Cl included in the perovskite layer increased carrier lifetime and mobility, and a 2T tandem cell was obtained with 27% efficiency [14]. Sarker et al. achieved an efficiency of 28.71% by using $MAGeI_3$ absorber on Si (with optimization of the absorber's thickness, work function, and bulk and interface defects) [2]. Islam et al. obtained an efficiency of 28.53%, with the lead-free compound of $CsSn_{0.5}Ge_{0.5}I_3$, and with the structure of $MAPbI_3$ on Si (with Cu_2O as a HTL and TiO_2 as the ETL); and an improved efficiency of 32.29% was accomplished [1]. Cherif and Sammouda presented a structure consisting of three cells (two perovskite cells with bandgaps of 1.8 eV and 1.45 eV respectively, on a single-crystal silicon cell) and achieved an efficiency of 34.27% [15].

2. Simulations and procedures

In this work, a three-cell perovskite-on-Si structure based on the monolithic 2T structure is designed and simulated. Numerical simulation was done using the Solar Cell Capacitor Simulator (SCAPS) 1D software under standard conditions of AM 1.5 solar spectrum and at a temperature of 300 K. In the SCAPS simulations, the materials input parameters were based on the experimental and theoretical data reported in the literature [1, 16], as listed in Tables 1 and 2. Specific parameters of individual cells are given in Table 3.

By entering the thickness and absorption coefficient of each of the cell layers in the MatLab software, the transmitted light spectra of the top and middle cells (i.e. the filtered spectra to be radiated to the next cell) were obtained.

3. Results and discussions

First, we simulated the $MAPbI_3$ cell based on the parameters given in Tables 1, 2 and 3. Then, by changing the HTL layer from Cu_2O to CuSCN (because it is more conductive and more transparent than Cu_2O) in the $MAPbI_3$ cell, the current density was improved and the cell efficiency was increased significantly. The J/V diagram of the $MAPbI_3$ cells with the two HTLs of $Cu2_O$ and CuSCN are compared in Fig. 1. The results (given in Table IV) compare the values

Table 1. Parameters used in the SCAPS simulations; the data were taken from the published articles.

Parameter	NiO	$Cs_2AgBi_{0.75}$	PCBM	SnO_2	Cu_2O	CuSCN	$MAPbI_3$	TiO_2	Si
Bandgap (eV)	3.6	1.8	2	3.5	2.17	3.7	1.55	3.26	1.12
Relative permittivity	11.7	6.5	3.9	9	7.11	10	10	10	11.9
Electron affinity (eV)	1.8	3.58	4	4	3.2	1.7	3.93	4.2	4.05
Electron mobility ($cm^2/V.s$)	1×10^{-3}	2	0.02	100	200	100	1	100	1400
Hole mobility ($cm^2/V.s$)	1×10^{-3}	2	0.02	25	80	25	1	25	450
Conduction Band Density of States $N_c(cm^{-3})\times10^{17}$	2500	22	117	22	20.2	220	27.5	2	289
Valence Band Density of States N_v $(cm^{-3})\times10^{17}$	2500	2180	42	180	110	18	39	6	104

Table 2. Defect characteristics in the solar cell layers. The data were taken from the published articles.

Defect location	Total density (cm^{-3})	Defect energy level above E_v (eV)	Defect type	Capture cross section of electrons (cm^{-2})	Capture cross section of holes (cm^{-2})
$MAPbI_3$,bulk	1×10^{15}	0.6	Neutral	1×10^{-15}	1×10^{-14}
$Cs_2AgBi_{0.75}Sb_{0.25}Br_6$, bulk	2.5×10^{13}	0.6	Neutral	2×10^{-14}	2×10^{-14}
CuSCN/$MAPbI_3$ interface	1×10^{9}	0.6	Acceptor	1×10^{-18}	1×10^{-19}
Cu_2O/$MAPbI_3$ interface	1×10^{15}	0.6	Neutral	1×10^{-19}	1×10^{-19}
$MAPbI_3$/TiO_2 interface	1×10^{15}	0.6	Neutral	1×10^{-19}	1×10^{-19}
NiO/$Cs_2AgBi_{0.75}Sb_{0.25}Br_6$ interface	1×10^{10}	0.6	Neutral	1×10^{-17}	1×10^{-17}
$Cs_2AgBi_{0.75}Sb_{0.25}Br_6$/PCBM interface	1×10^{10}	0.6	Neutral	1×10^{-17}	1×10^{-17}

Table 3. Specific parameters of each of the individual cells in the structure.

	Top cell				**Middle cell**					**Bottom cell**		
Parameter	NiO	$Cs_2AgBi_{0.75}Sb_{0.25}Br_6$	PCBM	TiO_2	Cu_2O	CuSCN	$MAPbI_3$	TiO_2	SnO_2	$Si_{(p+)}$	$Si_{(p)}$	$Si_{(n+)}$
Thickness (μm)	0.04	0.3	0.04	0.006	0.15	0.15	0.3	0.14	0.05	10	100	0.5
N_d (cm^{-3})	0	1×10^{13}	1×10^{18}	1×10^{17}	-	-	1×10^{17}	1×10^{17}	1×10^{15}	-	-	1×10^{20}
N_a (cm^{-3})	5×10^{17}	1×10^{17}	-	-	1×10^{18}	1×10^{18}	1×10^{9}	-	-	2.2×10^{20}	2.2×10^{16}	-

obtained from the simulations with the results reported in the literature. The structure of the three cells in the designed tandem structure are shown in Fig. 2. The NiO (in the top cell) and CuSCN (in the middle cell) act as the HTLs; and PCBM and TiO_2 (in the top cell) and TiO_2 plus SnO_2 (in the middle cell) act as the ETLs, respectively. Each of the $MAPbI_3$, $Cs_2AgBi_{0.75}Sb_{0.25}Br_6$, and single-crystal Si cells were simulated separately; their J/V characteristics under AM 1.5 condition, are shown in Fig. 3.

The efficiency of the $Cs_2AgBi_{0.75}Sb_{0.25}Br_6$ cell (with 300 nm absorber thickness) was 14.32%; for the $MAPbI_3$ cell (with 300 nm absorber thickness) the efficiency was 25.09%, and for the Si cell (with 100 μm thick p-substrate) it was 25.22%, respectively. These assured that the results were close to those reported in the literature, as compared in Table 4. in the designed tandem structure, the absorber layer of the top $Cs_2AgBi_{0.75}Sb_{0.25}Br_6$ cell had a bandgap of 1.8 eV, the bandgap of the $MAPbI_3$ in the middle cell was 1.55 eV, and the bottom cell of C-Si had a bandgap of 1.12 eV. Photons with energies smaller than the absorbing bandgap

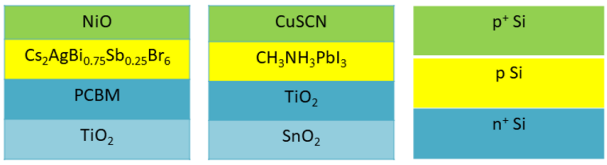

Figure 2. Schematic diagram of structures of the top, middle, and bottom cells (from left to right) in the designed tandem structure. Layer thicknesses are not to scale.

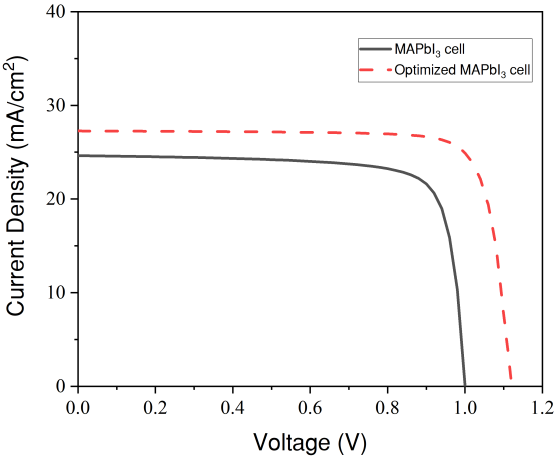

Figure 1. Comparison of J-V diagram of MAPbI3 cell (with Cu_2O as HTL) and the optimized MAPbI3 cell (with CuSCN as HTL).

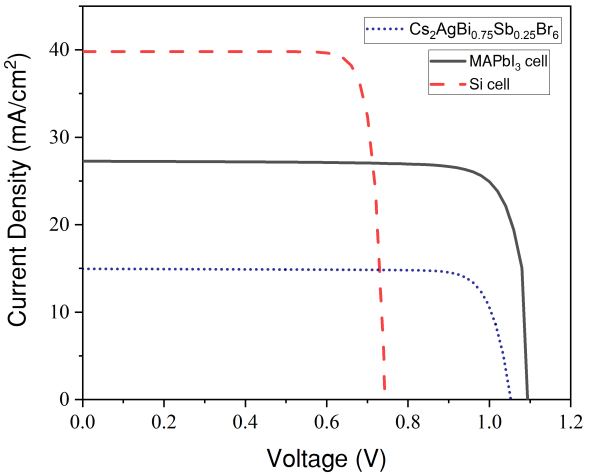

Figure 3. The independent J/V characteristics of the three individual cells in the tandem structure.

Table 4. Defect characteristics in the solar cell layers. The data were taken from the published articles.

Absorber material	VOC (V)	J_{SC} (mA/cm^2)	FF (%)	PCE (%)	Reference
$Cs_2AgBi_{0.75}Sb_{0.25}Br_6$	1.114	15.80	84.70	15.37	Kumar et al., 2021 [17]
$Cs_2AgBi_{0.75}Sb_{0.25}Br_6$	1.14	14.95	83.96	14.32	**This work**
$MAPbI_3$-(Cu_2O)	1.113	23.35	76.98	20.01	Islam et al., [1]
$MAPbI_3$-(Cu_2O)	1	24.63	79.29	19.53	**This work**
$MAPbI_3$-(CuSCN)	1.19	25.61	87.81	26.74	Raoui et al., [18]
$MAPbI_3$-(CuSCN)	1.14	27.26	80.11	25.09	**This work**
C-Si	0.76	40.04	85.47	25.96	Yoshikawa et al., 2017 [19]
C-Si	0.74	39.79	85.26	25.22	**This work**

energy pass through the top cell; part of that spectrum is absorbed by the middle cell; and finally, the transmitted photons will be partly absorbed by the bottom cell. Therefore, these cells can be considered as three diodes connected in series. The upper $Cs_2AgBi_{0.75}Sb_{0.25}Br_6$ cell was exposed to the AM 1.5 standard spectrum, and the spectrum passing through the upper cell (which was considered as the light source for the lower cell) was calculated using the following equation (This method is widely used in simulation of tandem cells using SCAPS software).

$$S(\lambda) = S_0(\lambda).\exp(\sum_{i=1}^{4} -\alpha_{mat_i}(\lambda)d_{mat_i}) \qquad (1)$$

where S_0 is the AM 1.5 spectrum, and S is the output (i.e. filtered) spectrum of the top cell, which is obtained by using the absorption coefficients ($\alpha_{mat\,i}$)and film thicknesses ($d_{mat\,i}$)of the top cell layers. In the SCAPS software, this filtered spectrum is defined as the light source radiated to the middle cell. The spectrum of the light reaching the bottom Si cell was similarly calculated (using the above equation). Fig. 4 shows the structure of the designed tandem solar cell and the light spectrum of AM1.5 and the spectra filtered by the $Cs_2AgBi_{0.75}Sb_{0.25}Br_6$ and $MAPbI_3$ cells. The condition of current-matching between the three cells in the tandem structure was obtained by optimization of the three individual cells. That is, the thicknesses of the absorber layers were adjusted so that an equal current was produced in all three cells. Finding the optimal value for the absorber layer thickness of the middle cell was important; because it affects the lower cell's current directly; i.e. increasing the thickness of the absorber layer in the middle cell reduces the amount of light reaching the lower cell (and hence, results in a lower current produced by the lower cell). Alternatively, a reduction in the thickness of the absorber layer of the

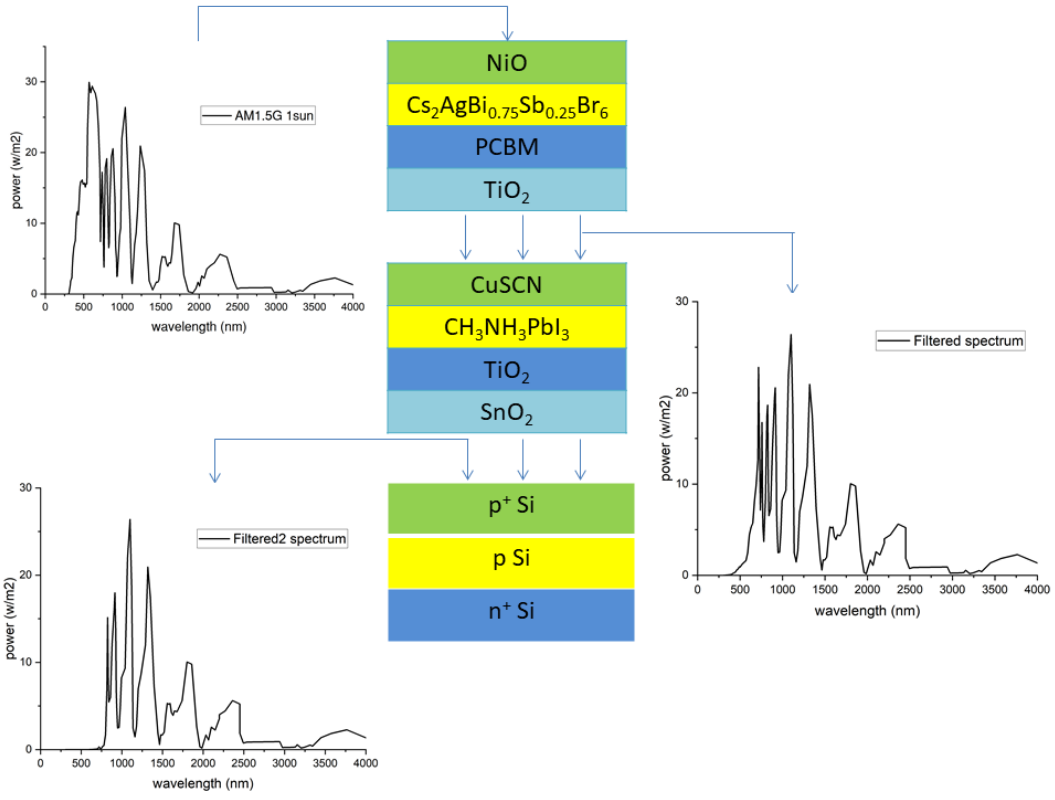

Figure 4. The structure of the designed tandem structure and the light spectra of AM1.5 and the ones filtered by the middle and bottom cells.

Table 5. Specifications of the three single cells in the designed structure and the final tandem cell.

Cell	V_{oc} (V)	J_{sc} (mA/cm^2)	FF	PCE
$Cs_2AgBi_{0.75}Sb_{0.25}Br_6$	1.14	14.95	83.96	14.32
$MAPbI_3$	0.99	14.93	78.92	19.06
c-Si	0.71	14.97	84.87	21.51
Tandem	2.84	14.95	0.91	38.9

middle cell will result in a lower current in the middle cell. Therefore, the three cells were optimized for a current of close to 14.9 mA. With this current, the optimum thickness values for $Cs_2AgBi_{0.75}Sb_{0.25}Br_6$ and $MAPbI_3$ layers were found to be 300 nm and 550 nm respectively.
Consequently, the current density (Jsc) of the tandem cell was 14.95 mA and its Voc was equal to the sum of the open circuit voltages of the three individual cells i.e. 2.84 V. The current-voltage characteristics of the three single cells and the tandem cell is shown in Fig. 5, and the values of Jsc, Voc, FF, and PCE are given in Table 5. As the above Table shows, a power conversion efficiency of 38.9% is obtained for the designed tandem structure, which indicates a cosiderable improvement.

4. Conclusion

A two-terminal three-junction perovskite/perovskite/Si tandem solar cell is designed and optimized for enhancement of the power conversion efficiency, using the SCAPS software. The filtered spectrum through the upper cell was obtained and used for the illumination of the middle cell, and similarly, the transmitted spectrum from the middle cell was used for the illumination of the bottom cell. The current-matching conditions between the three cells were realized by changing the absorber-layer thicknesses of the two perovskite cells. The final PCE value obtained was 38.9%, which shows a significant improvement.
Despite of attractive advantages (such as low cost and high efficiencies) the cells based on the perovskite materials have some drawbacks as well. These include toxicities of the materials, device hysteresis, and durability of the perovskite materials (when directly exposed to humidity in the environment). These are the main challenges that should be addressed before mass production stage of the perovskite cells.
To remove toxicity, there has been some research done on substitution of Cu instead of Pb in perovskite layers [20]. The other major problem is the long-term stability of the perovskite cells. This is due to the sensitivity of the hybrid organic/inorganic perovskite cells to moisture in the environment, which by proper packaging configuration of the device, this can be considerably reduced. There are other factors affecting the performance of these cells, such as the device operating temperature and large-area uniformity of the thin film layers [21, 22], which are common parameters among other thin-film cells as well.

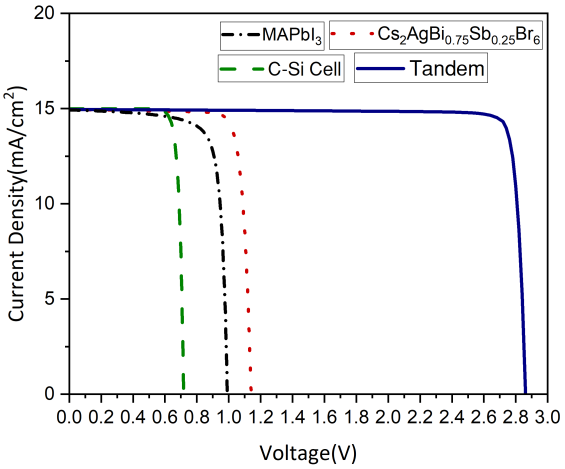

Figure 5. The J/V characteristics of the three single cells and the tandem cell.

Authors contributions
All authors have contributed equally to prepare the paper.

Availability of data and materials
The data that support the findings of this study are available from the corresponding author upon reasonable request.

Conflict of interests
The authors declare that they have no known competing financial interests or personal relationships that could have appeared to influence the work reported in this paper.

References

[1] T. Islam, R. Jani, A. F. Islam, K. Shorowordi, S. Chowdhury, S. S. Nishat, and S. Ahmed. "**Investigation of $CsSn_{0.5}Ge_{0.5}I_3$-on-Si tandem solar device utilizing SCAPS simulation**.". *IEEE J. Trans. Electron Devices*, 68(618), 2021. DOI: https://doi.org/10.1109/TED.2020.3045383.

[2] S. Sarker, T. Islam, A. Rauf, H.A. Jame, R. Jani, S. ISLAM, S.S. Nishat, K. Shorowordi, and S. Ahmed. "**A SCAPS simulation investigation of non-toxic $MAGeI_3$-on-Si tandem solar device utilizing monolithically integrated (2-T) and mechanically stacked (4-T) configurations**.". *Sol. Energy*, 225(471), 2021. DOI: https://doi.org/10.1016/j.solener.2021.07.057.

[3] G. Conibeer. "**Third-generation photovoltaics**.". *Mater. Today*, 10(42), 2007. DOI: https://doi.org/10.1016/S1369-7021(07)70278-X.

[4] L. Lin, P. Li, L. Jiang, Z. Kang, Q. Yan, H. Xiong, S. Lien, P. Zhang, , and Y. Qiu. "**Boosting efficiency up to 25% for HTL-free carbon-based perovskite solar cells by gradient doping using SCAPS simulation**.". *Sol. Energy*, 215(328), 2021. DOI: https://doi.org/10.1016/j.solener.2020.12.059.

[5] L.A. Frolova, A.I. Davlethanov, N.N. Dremova, I. Zhidkov, A.F. Akbulatov, E.Z. Kurmaev, S.M. Aldoshin, K.J. Stevenson, and P.A. Troshin. "**Efficient and stable $MAPbI_3$-based perovskite solar cells using polyvinylcarbazole passivation**.". *J. Phys. Chem. Lett*, 11(16):pp. 6772, 2020. DOI: https://doi.org/10.1021/acs.jpclett.0c01776.

[6] J. P. Mailoa, C. D. Bailie, E. C. Johlin, E. T. Hoke, A. J. Akey, W. H. Nguyen, M. D. McGehee, and T. Buonassisi. " **A 2-terminal perovskite/silicon multijunction solar cell enabled by a silicon tunnel junction**.". *Appl. Phys. Lett*, 206(121105), 2015. DOI: https://doi.org/10.1063/1.4914179.

[7] S. Albrecht, M. Saliba, J. P. Correa Baena, F. Lang, L. Kegelmann, M. Mews, L. Steier, A. Abate, J. Rappich, L. Korte, R. Schaltmann, M. Khaja Nazeeruddin, A. Hagfeldt, M. Grätzel, and B. Rech. "**Monolithic perovskite/siliconheterojunction tandem solar cells processed at low temperature**.". *Energy Environ. Sci*, 9(81), 2016. DOI: https://doi.org/10.1039/C5EE02965A.

[8] J. Werner, C. H. Weng, A. Walter, L. Fesquet, J.P. Seif, S. De Wolf, B. Niesen, and C. Ballif. "**efficient monolithic perovskite/silicon tandem solar cell with cell area>1 cm^2**.". *J. Phys. Chem. Lett*, 7(161), 2016. DOI: https://doi.org/10.1021/acs.jpclett.5b02686.

[9] H. Shen, S. T. Omelchenko, D. A. Jacobs, S. Yalamanchili, Y. Wan, D. Yan, P. Phang, t. Doung, Y. Yin, C. Samundsett, J. Peng, N. Wu, T. P. White, G. Andersson, N. S. Lewis, and K. R. Catchpole. "**In situ recombination junction between p-Si and TiO_2 enables high-efficiency monolithic perovskite/Si tandem cells**. ". *Sci. Adv*, 4(eaau9711), 2018. DOI: https://doi.org/10.1126/sciadv.aau9711.

[10] K. A. Bush, A. F. Palmstrom, Z. J. Yu, M. Boccard, R. Cheacharoen, J. P. Mailoa, D. P. McMeekin, R. L. Z. Hoye, C. D. Bailie, T. Leijtens, I. M. Peters, M. C. Minichetti, N. Rolston, R. Prasanna, S. Sofia, D. Harwood, W. Ma, F. Moghadam, H.J. Sanith, T. Buonassisi, Z. C. Holan, S. F. Bent, and M.D. McGehee. "**23.6%-efficient monolithic perovskite/silicon tandem solar cells with improved stability**.". *Nat. Energy*, 2:pp. 17009, 2017. DOI: https://doi.org/10.1038/nenergy.2017.9.

[11] K. A. Bush, S. Manzoor, K. Frohna, Z. J. Yu, J. A. Raiford, A. F. Palmstrom, H. P. Wang, R. Prasanna, S. F. Bent, Z. C. Holman, and M.D. "**McGehee, minimizing current and voltage losses to reach 25% efficient monolithic two-terminal perovskite–silicon tandem solar cells**.". *ACS. Energy Lett*, 3:pp. 2173, 2018. DOI: https://doi.org/10.1021/acsenergylett.8b01201.

[12] F. Sahli, B. A. Kamino, J. Werner, M. Bräuninger, B. Paviet-Salomon, L. Barraud, R. Monnard, J. P. Seif, A. Tomasi, Q. Jeangros, A. Hessler-Wyser, S. De Wolf, M. Despeisse, S. Nicolay, B. Niesen, and C. Ballif. "**Improved optics in monolithic perovskite/silicon tandem solar cells with a nanocrystalline silicon recombination junction**.". *Adv. Energy Mater*, page pp. 1701609, 2017. DOI: https://doi.org/10.1002/aenm.201701609.

[13] F. Sahli, J. Werner, B. A. Kamino, R. Monnard, B. Paviet-Salomon, L. Barraud, L. Ding, J. J. Diaz Leon, D. Sacchetto, G. Cattaneo, M. Despeisse, M. Boccard, S. Nicolay, Q. Jeangros, B. Niesen, and C. Ballif. "**Fully textured monolithic perovskite/silicon tandem solar cells with 25.2% power conversion efficiency**.". *Nat. Mater*, 17(820), 2017. DOI: https://doi.org/10.1038/s41563-018-0115-4.

[14] J. Xu, C. C. Boyd, Z. J. Yu, A. F. Palmstrom, D. J. Witter, B. W. Larson, R. M. France, J. Werner, S. P. Harvey, E. J. Wolf, W. Weigand, S. Manzoor, M. F. A. M. v. Hest, J. J. Berry, J. M. Luther, Z. C. Holman, and M. D. McGehee. "**Triple-halide wide–band gap perovskites with suppressed phase segregation for efficient tandems**.". *Science*, 367(1097), 2020. DOI: https://doi.org/10.1126/science.aaz5074.

[15] F. E. Cherif and H. Sammouda. "**Optoelectronic simulation and optimization of tandem and multi-junction perovskite solar cells using concentrating photovoltaic systems**.". *Energy Rep*, 7.

[16] J. Madan, Shivani, R. Pandey, and R. Sharma. "**Device simulation of 17.3% efficient lead-free all-perovskite tandem solar cell**.". *Sol. Energy*, 197(212), 2020. DOI: https://doi.org/10.1016/j.solener.2020.01.006.

[17] A. Kumar, Sh. D. Saurabh, and H. Sharma. "**Perovskite-CIGS materials based tandem solar cell with an increased efficiency of 27.5%. mater**.". *Today. Proceedings*, 45(5047), 2021. DOI: https://doi.org/10.1016/j.matpr.2021.01.565.

[18] Y. Raoui, H. Ez-Zahraouy, N. Tahiri, O. E. Bounagui, S. Ahmad, and S. Kazim. "**Performance analysis of $MAPbI_3$ based perovskite solar cells employing diverse charge selective contacts: simulation study**.". *Sol. Energy*, 193(948), 2019. DOI: https://doi.org/10.1016/j.solener.2019.10.009.

[19] K. Yoshikawa, H. Kawasaki, W. Yoshida, T. Irie, K. Konishi, K. Nakano, T. Uto, D. Adachi, M. Kanematsa, H. Uzo, and K.Yamamoto. "**Silicon heterojunction solar cell with interdigitated back contacts for a photoconversion efficiency over 26%**.". *Nat. Energ*, 2(17032), 2017. DOI: https://doi.org/10.1038/nenergy.2017.32.

[20] M. Aamir, M. Sher, and J. Akhtar. "**Synthesis of lead free hybrid copper halide perovskite nanosheets: structural and optical properties**.". *Results in Optics*, 13(100562), 2023. DOI: https://doi.org/10.1016/j.rio.2023.100562.

[21] J. Zhao, M. Hou, Y. Wang, R. Wang, J. Zhang, H. Ren, G. Hou, Y. Ding, Y. Zhao, and X. Zhang. "**Strategies for large-scale perovskite solar cells realization**.". *Organic Electronics*, 122(106892), 2023. DOI: https://doi.org/10.1016/j.orgel.2023.106892.

[22] A. Agresti, F. Giacomo, S. Pescetelli, and A. Carlo. "**Scalable deposition techniques for large-area perovskite photovoltaic technology: A multi-perspective review**.". *Nano Energy*, 122(109317), 2024. DOI: https://doi.org/10.1016/j.nanoen.2024.109317.